NASA CR-134212
ERIM 198200-1-F

MULTI-FREQUENCY FINE RESOLUTION IMAGING RADAR INSTRUMENTATION AND DATA ACQUISITION

by

Robert A. Rendleman, et al.

Radar and Optics Division

ENVIRONMENTAL RESEARCH INSTITUTE OF MICHIGAN
FORMERLY WILLOW RUN LABORATORIES.
THE UNIVERSITY OF MICHIGAN

FEBRUARY 1974

prepared for

NATIONAL AERONAUTICS AND SPACE ADMINISTRATION
Johnson Space Center
Houston, Texas 77058
Contract NAS 9-11306

NOTICES

Sponsorship. The work reported herein was conducted by the Environmental Research Institute of Michigan for the National Aeronautics and Space Administration, Johnson Space Center, Houston, Texas 77058, under Contract NAS 9-11306. Carl O. McClenny/TF is Technical Initiator. Contracts and grants to the Institute for the support of sponsored research are administered through the Office of Contracts Administration.

TECHNICAL REPORT STANDARD TITLE PAGE

1. Report No. NASA CR-ERIM 198200-1-F	2. Government Accession No.	3. Recipient's Catalog No.
4. Title and Subtitle MULTI-FREQUENCY FINE RESOLUTION IMAGING RADAR INSTRUMENTATION AND DATA ACQUISITION		5. Report Date February 1974 6. Performing Organization Code
7. Author(s) R. A. Rendleman, E. B. Champagne, J. E. Ferris, C. L. Liskow, J. M. Marks, R. J. Salmer		8. Performing Organization Report No. ERIM 198200-1-F
9. Performing Organization Name and Address Environmental Research Institute of Michigan Radar and Optics Division P.O. Box 618 Ann Arbor, MI 48107		10. Work Unit No. 11. Contract or Grant No. NAS 9-11306 13. Type of Report and Period Covered Final Report—1 June 1970 through 15 January 1973
12. Sponsoring Agency Name and Address National Aeronautics and Space Administration Johnson Space Center Houston, Texas 77058		14. Sponsoring Agency Code

15. Supplementary Notes

Carl O. McClenny/TF is Technical Initiator.

16. Abstract

Development of a dual-polarized L-band radar imaging system to be used in conjunction with the present dual-polarized X-band radar is described. The work was done under contract with NASA's Johnson Space Center in Houston by the Radar and Optics Division of the Environmental Research Institute of Michigan, formerly the Willow Run Laboratories of The University of Michigan. The contract number is NAS 9-11306. The effort was intended to provide a dual-band capability with minimum cost and minimum technical risk by taking advantage of the existence of most of the technically difficult portions of the airborne equipment already installed in the Institute's C-46 aircraft. The technique used called for heterodyning the transmitted frequency from X-band to L-band and again heterodyning the received L-band signals back to X-band for amplification, detection, and recording.

17. Key Words	18. Distribution Statement
Multi-frequency radar Fine resolution imaging radar Dual-polarized radar imaging system Heterodyning	Initial distribution is listed at the end of this document.

19. Security Classif. (of this report)	20. Security Classif. (of this page)	21. No. of Pages	22. Price
UNCLASSIFIED	UNCLASSIFIED	44	

PREFACE

This document describes the technical results obtained under Contract NAS9-11306, "Multi-Frequency Fine Resolution Imaging Radar Instrumentation and Data Acquisition." This contract between NASA and The University of Michigan was initially executed in June 1970, and subsequently was amended; the period of performance ended 15 January 1973. The responsibility for the technical performance under this contract was assigned within the University to the Willow Run Laboratories of the Institute of Science and Technology. On January 1, 1973, the University transferred the contracts, personnel and facilities of the Willow Run Laboratories to the Environmental Research Institute of Michigan (ERIM), a newly formed not-for-profit corporation in the State of Michigan. This ERIM report, which satisfies the contractual requirement under NAS9-11306 for a final report, was prepared by the Radar and Optics Division of ERIM. Robert A. Rendleman served as the Principal Investigator for the program. The Environmental Research Institute of Michigan number for this report is 198200-1-F.

The authors gratefully acknowledge the contributions made by ERIM's James W. Freese, Robert F. Rawson, and Frank L. Smith.

CONTENTS

FIGURES

TABLES

MULTI-FREQUENCY FINE RESOLUTION IMAGING RADAR
INSTRUMENTATION AND DATA ACQUISITION

FINAL REPORT
1 June 1970 Through 15 January 1973

1
INTRODUCTION

The potential applicability of sidelooking airborne radar (SLAR) to earth-resource survey has been under investigation since the mid-1960's, at which time imagery from early "noncoherent" SLAR's became available to the scientific community. Preliminary results were presented at the Remote Sensing Symposium as early as 1964. The radars used to generate the imagery used in the early evaluation of applicability for earth-resource survey have the property that, although relatively fine resolution could be maintained in one dimension of the image (the "range" dimension, perpendicular to the flight path of the radar-bearing aircraft), performance in the along-track dimension deteriorated as the slant range from the aircraft to the terrain region being observed increased. In systems of the noncoherent class, the along-track resolution ρ_x is on the order of

$$\rho_x \simeq \frac{\lambda}{D} R$$

where

- λ is the operating wavelength
- D is the size of the antenna carried on the aircraft, and
- R is the slant range to the terrain region of interest

Although the early imagery achieved ρ_x values fine enough to command attention within the user

disciplines, this was the result of operating at relatively short range and with relatively short wavelengths on the order of 1 to 3 cm. The resolution achieved at these short ranges could not be held at the long operating ranges envisioned for NASA spacecraft, and even at short ranges it was not feasible to achieve fine ρ_x at the longer wavelengths which otherwise appeared attractive from a science/user point of view.

The solution to this apparent impasse lay in the synthetic-aperture radar (SAR) concept, which had been under investigation under DoD sponsorship since the early 1950's, but was subject to security regulations. These sidelooking radar systems employed coherent radars and associated data storage and processing systems to achieve fine along-track resolution ρ_x. In theory, a focused SAR system can achieve resolution $\rho_x \approx D/2$, independent of slant range R and operating wavelength D; in practice, uncompensated errors induced in the radar by the storage/processor system, by the motion of the aircraft, and by atmospheric turbulence serve to limit the resolution which is actually realized. Declassification of certain aspects of SAR technology was underway by 1966, and was followed by declassification of substantial quantities of SAR imagery starting in 1970. This initial declassification, along with the ability of SAR's to generate comparably fine resolutions at different operating wavelengths at long operating ranges, opened the door for NASA to seriously explore the concept of multispectral imaging radar for spacecraft as well as aircraft operation. It was decided for reasons of cost and complexity to limit the hardware program to the use of two wavelengths, but to equip the receiving system with two channels for each wavelength, one to respond to reflected signals having the same polarization as the linearly polarized transmitted signal, and a second to respond to the cross-polarized reflected signal. Because we wished to capitalize on the extensive experience in both the SAR hardware area and the image interpretation area which was available at 3 cm (X-band), the decision was made to set one operating wavelength at 3 cm for the initial exploratory program. In order to guarantee that the second wavelength would respond to a substantially different scale of surface roughness than would the X-band signal, it was decided to try and hold these an order of magnitude apart. The decision to select 30 cm (L-band) as the second wavelength reflected the fact that some of the discrimination desired for earth-resource survey missions would benefit from the degree of foliage penetration available in this spectral region, as well as reflecting the availability of component hardware. The general program plan had the following steps associated with it.

a) Fabricate a dual-frequency, dual-polarization SAR system which could operate on one frequency in a given flight, but which could be reconfigured on a day-to-day basis to collect data on the second frequency;

b) Collect limited two-frequency data in the mode described in (a), exercise the optical correlator to generate images at the two wavelengths and provide data to geoscience users specified by NASA;

c) Add a multiplexing feature to the radar to permit simultaneous generation of radar data at the two frequencies.

Steps (a) and (b) of this program plan were funded through this contract; step (c) was funded later through a separate contract, NAS9-12967, which is reported elsewhere.

The contract, as originally executed in June 1970, covered step (a) described above. An L-band radar was to be designed and fabricated, and then installed in a University of Michigan aircraft which had previously been equipped with an X-band SAR under DoD support. The L-band radar components were to be compatible with the existing airborne recorders as well as the navigation and motion compensation systems in the aircraft. The recorded data format was to be similar to the existing X-band format in order to permit optical processing of the recorded L-band radar data in The University of Michigan optical processors. The contract provided for a flight demonstration of the L-band radar system using the newly installed L-band electronics package and an L-band antenna. The flight test was to include operation of the airborne imaging radar system at L- and X-bands on alternate days in order to image selected sections of terrain at both radar wavelengths with only a one-day time difference. A contract amendment in December 1971 added funds to exercise the two-frequency radar to image a variety of terrain types. At Manned Space Center instruction, funds were transferred from another NASA-sponsored effort at The University of Michigan (NAS9-9784) to allow optical processing of a small portion of these recorded data. Finally, in December 1972, a final increment was added to the funding of the contract to allow additional optical processing.

The X-band (3 cm) imaging radar already installed in a University of Michigan aircraft utilizes modern techniques of pulse compression in two dimensions in order to provide fine-resolution radar imagery of a terrain swath parallel to the flight path. With this equipment, radar imagery of the terrain is obtained at a rate of about 500 square miles per hour of flight time. The received radar signal recorded during flight is processed in a ground-based optical processor and the resulting output imagery is presented as a strip map on 70 mm photographic film. This imagery can be viewed directly, projected on a screen, or photographic prints can be made. It was felt that these same techniques could be applied to provide L-band (30 cm) radar imagery with fine resolution in the same photographic form as the X-band imagery. It was thought also that much of the auxiliary equipment required in the aircraft for fine-resolution radar imaging could be used with radars operating at different wavelengths, and that, by maintaining a similar recording format, the same optical processor would be applicable. These considerations supported the decision to use The University of Michigan airborne radar system as a convenient base upon which to expand the available wavelength coverage by adding only the required L-band components.

The proposed dual-frequency imaging radar utilizes the unusual technique of retaining most of the X-band system but converting the transmitter output signal to L-band before radiating it and reconverting the L-band echo signals to X-band for amplification and detection. This concept takes advantage of the technically-complex existing parts of the X-band radar for pulse generation, timing, and synchronous detection as well as motion compensation, recording, and data processing. As a result, the required new development work was confined largely to down-conversion, amplification at L-band, a new L-band antenna, and up-conversion.

The proposed scheme was intended to allow X-band data to be gathered one day followed by an overnight change to the L-band antenna and the addition of up- and down-converters; then, L-band data could be gathered the following day. In actuality, the new L-band antenna was designed so that it could be mounted in the radome along with the existing dual-polarized X-band antenna. Frequency change could thus be performed in the air in about twenty minutes. Other than this, all of the other system modifications were engineered as proposed. Successful image gathering at both wavelengths has been demonstrated both experimentally and semi-operationally at field sites remote from the radar's home base.

2
ELECTRONICS

Two distinct design approaches were considered before the final L-band radar electronics evolved. These are discussed briefly in the following paragraphs along with the reasoning behind the final choice. A more complete description of the final system is then presented.

Starting with an existing X-band system, one would naturally consider first the technique of replacing each X-band device with its L-band counterpart. Two major problems arose in connection with this approach. First, many X-band devices do not have direct counterparts available at L-band. Secondly, since the frequency reduction from X- to L-band is almost an order of magnitude and the required bandwidth reduction is only two times, many of the L-band components would be required to operate over an increased percentage bandwidth. These two problems were ones in which the available personnel has little experience. Thus, although this approach could probably be made to work, it involved a time risk due to these problems that was deemed unacceptable. Therefore, this direct approach was abandoned.

Systems utilizing X-band intermediate frequencies and L-band radiation frequencies are not generally found in use and would seem to be pointless, at first glance. Having an X-band system,

however, one can conceive of changing the radiation frequency either up or down just prior to transmission and again just after reception in order to provide any desired radiated wavelength. Since systems with L-band intermediate frequency and X-band transmission are not uncommon, the necessary components are available. The heterodyne process is bilateral; ordinary mixers can be used. Accordingly, this approach was chosen because of the low risk factor.

The cost of the L-band imaging system was kept to an absolute minimum by building it as a converter to be added to the existing X-band system operated by The University of Michigan Radar and Optics Laboratory. A functional block diagram of the X-band radar with the L-band converter is shown in Fig. 1. To the left of the dotted box are most of the difficult and costly functions of the radar: broad-band pulse generation, motion compensation, data storage, received-signal amplification, stable local oscillator (STALO), and phase-coherent signal generation. Within the dotted box are only the L-band transmitter, circulator, receiver first stages, converters, and a dual-polarized antenna. The system outside the box is identical in both radar modes except for changes in (1) the bandwidth of the pulse generated in the sweep generator and (2) the scale factor of the motion compensation signal. In the L-band transmitter path, the broadband pulse generated at X-band is heterodyned down to L-band by beating it against STALO No. 2, whose frequency is the difference between the center frequencies of the X- and L-bands. After filtering, this L-band signal is amplified in a transistor amplifier, gated, then amplified further and transmitted as in the X-band transmitter. A 20-watt TWT and a 37-kilowatt TWT were cascaded in order to increase the power level for transmission. The 37-kilowatt tube was selected primarily because of its compatibility with the power supply and modulator used to operate the X-band 15-kilowatt transmitter. In addition, a parallel transmitter channel was provided (as shown in Fig. 1) for use as a spare and for testing. This channel consists of a 100-milliwatt transistor amplifier and a 5-kilowatt TWT. The 5-kilowatt TWT was selected primarily because of its compatibility with the power supply and modulator used to operate the X-band 1-kilowatt transmitter.

Antenna duplexing was accomplished by using a high-power coaxial circulator and a low-power diode limiter in the parallel-polarized receiver channel. In the cross-polarized receiver channel, a diode limiter was sufficient to protect the low-power amplifier from damage by the transmitter signal. The receiver in each of the two channels consists of an L-band transistor amplifier with 35 db gain and 4 db noise figure. At this point, the received signals are heterodyned back to X-band using the same STALO signal that was used in the transmitter down-conversion. A major oversight in the original system design occurred in this particular converter. The STALO signal used to heterodyne the received signals back to X-band leaked through the converter and, although outside the desired band, saturated the tunnel-diode amplifiers. This problem was difficult to isolate, but when understood was easily corrected by the addition of a bandpass filter. All additional amplification, signal conditioning, detection, and recording are performed in the X-band receivers and CRT-film data recorders in the normal manner, with the exception that the phase compensation for antenna lateral motion had to be

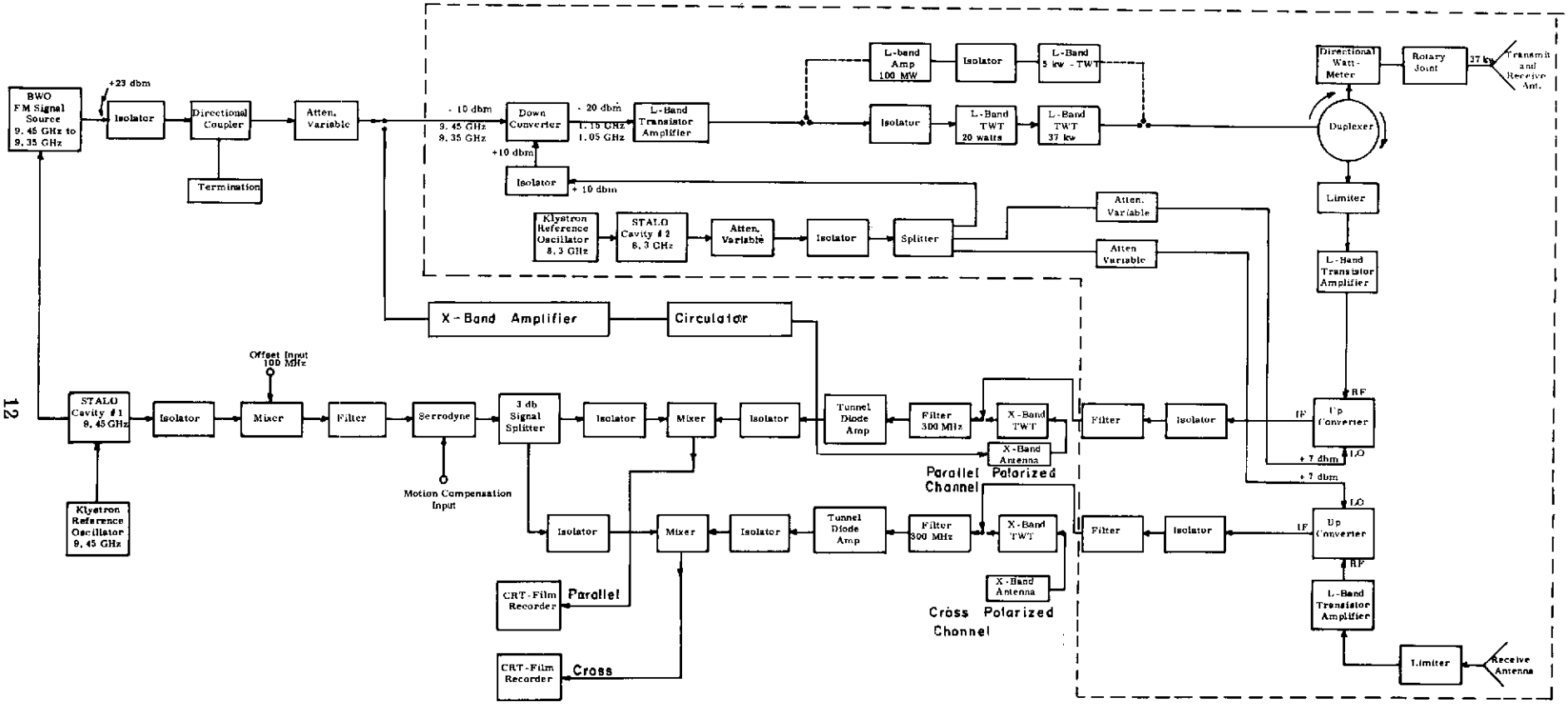

FIGURE 1. BLOCK DIAGRAM L-BAND RADAR

rescaled by the ratio of the X- to L-band wavelengths. This change was accomplished by changing the phase sensitivity of the serrodyne modulator (phase shifter).

A low-power-level system test was conducted early in the construction program utilizing the configuration outlined in Fig. 2. The purpose of the test was to determine if an X-band chirp signal of the required 100 MHz bandwidth could be down-converted to L-band and then up-converted to the original X-band frequency, all with adequate fidelity. In this test, a laboratory BWO was set up to generate an X-band chirp signal of the desired bandwidth and pulse length. This signal was then down-converted to L-band, amplified, and then up-converted to X-band. The original X-band chirp signal was synchronously detected and recorded on photographic film. The same signal after converting down and up was recorded in the same way. The two recorded signals were then pulse-compressed in an optical processor and the resulting optical images were examined to obtain a qualitative measure of the adequacy of the conversion operations. Figure 3 shows a chart recorder tracing of a photometric scan of these output images. It can be seen that both compressed pulses have essentially the same main lobe width, indicating that the frequency translations had not introduced significant degradation in the range resolution of the radar. Both compressed pulses have side lobe levels about 7 db below the main lobe. This level is not unexpected, since no attempt had been made to minimize the side lobe level in this experiment. However, it is important to note that the side lobe structures and level are similar in the two cases; thus, it can be concluded that none of the circuit components has introduced substantial phase or amplitude variations in the linear frequency-modulated pulse.

3
ANTENNAS

To satisfy the requirements of the dual-frequency radar program, two dual-polarized antenna systems were required, one for L-band and the other for X-band. The antennas that were employed have the characteristics listed in Table I.

The L-band antenna consists of seven dual-polarized log-periodic elements arrayed colinearly with the elements spaced eight inches center-to-center (See Fig. 4). The horizontally and vertically polarized arrays have separate but similar corporate feed structures which were fabricated employing strip-line techniques.

To satisfy the 50-Kw requirement, the strip-line corporate feed structures employ air dielectric. Each structure has a triangularly-shaped center conductor whose input impedence is 50 ohms and whose output impedence is 50/8 = 6.25 ohms. The input and output connectors consist respectively of one EIA 7/8-inch (50 ohm) connector and seven UG-58/U panel connectors. Details of the L-band dual-polarized antenna, including some test measurements, are presented in Appendix A.

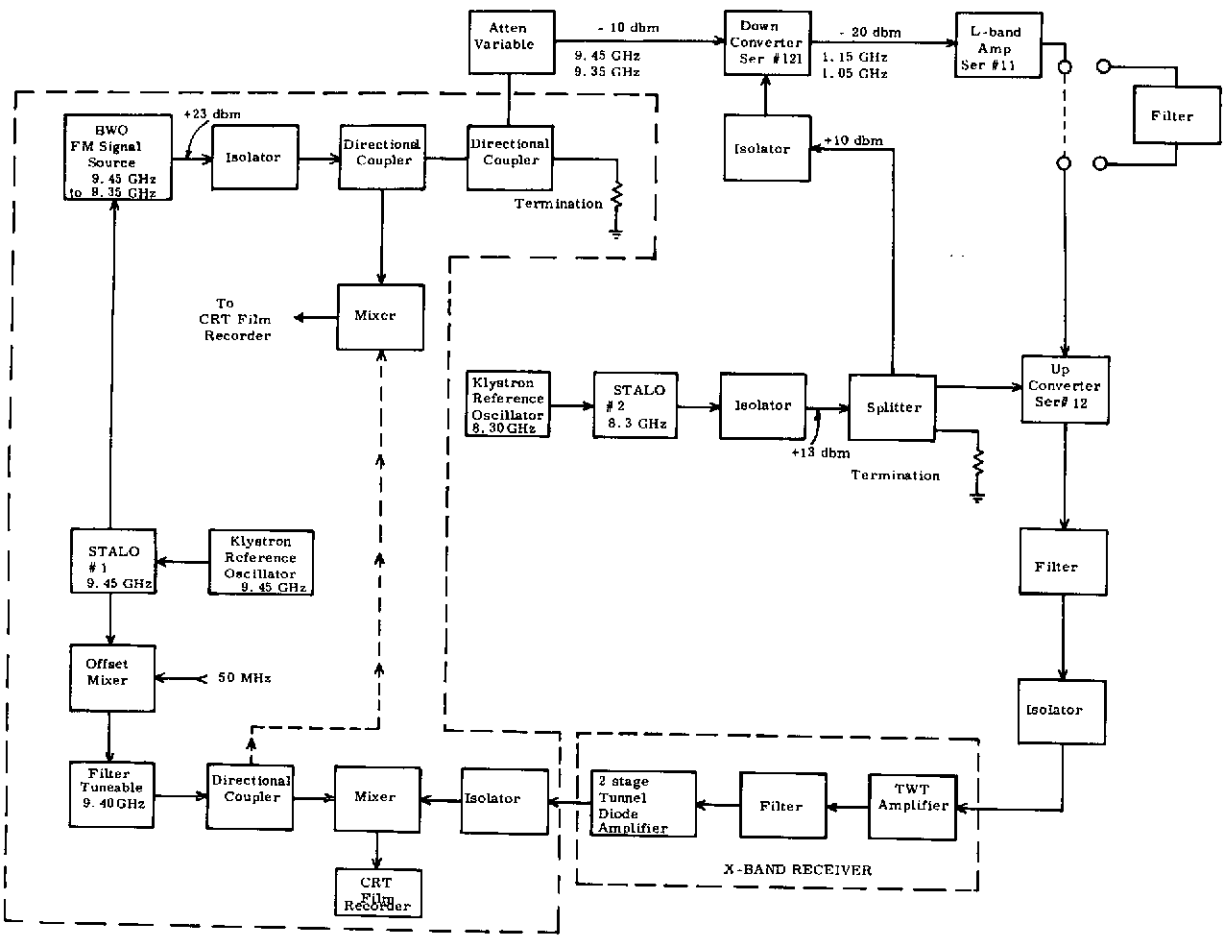

FIGURE 2. TEST – BLOCK DIAGRAM – X TO L TO X CONVERSION CONFIGURATION

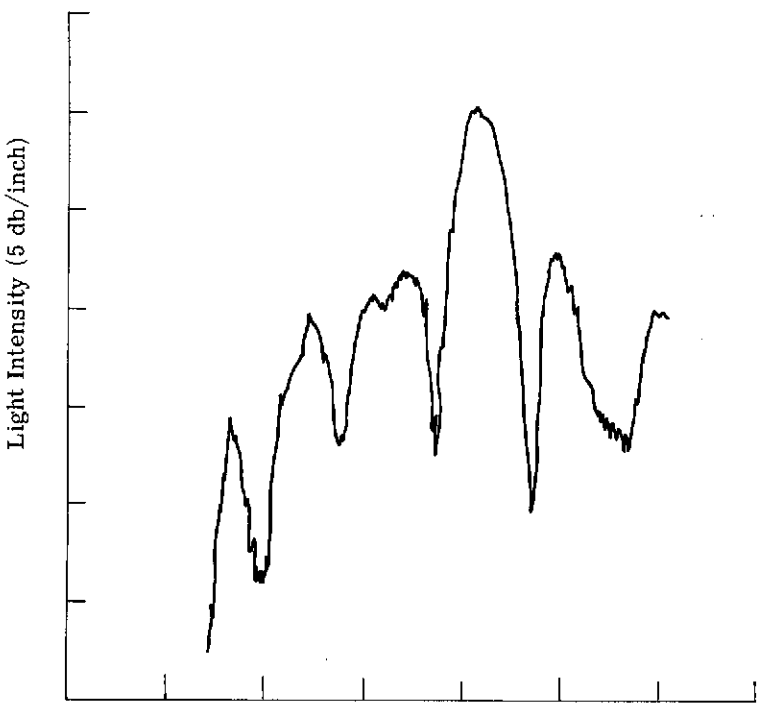

FIGURE 3A. COMPRESSED PULSE BEFORE HETERODYNING

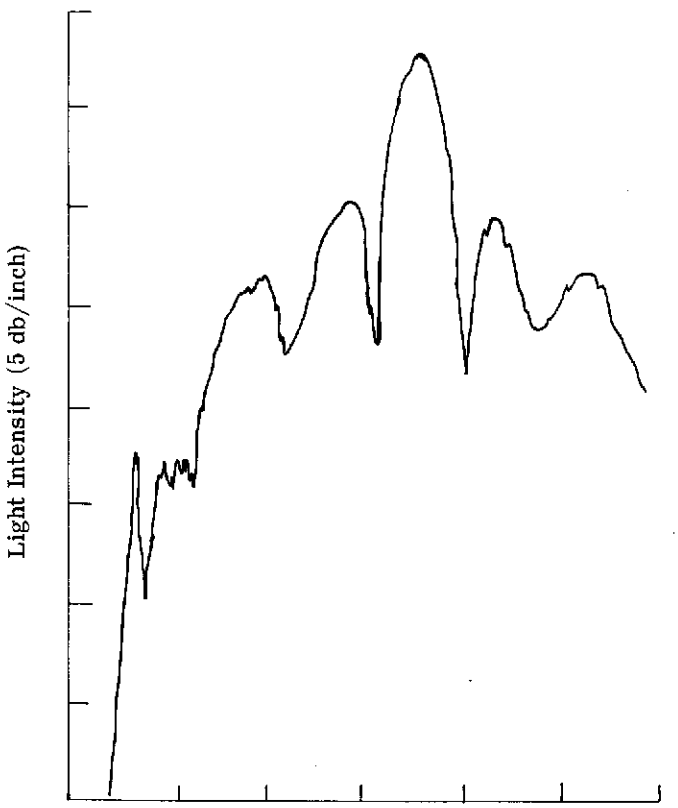

FIGURE 3B. COMPRESSED PULSE AFTER HETERODYNING

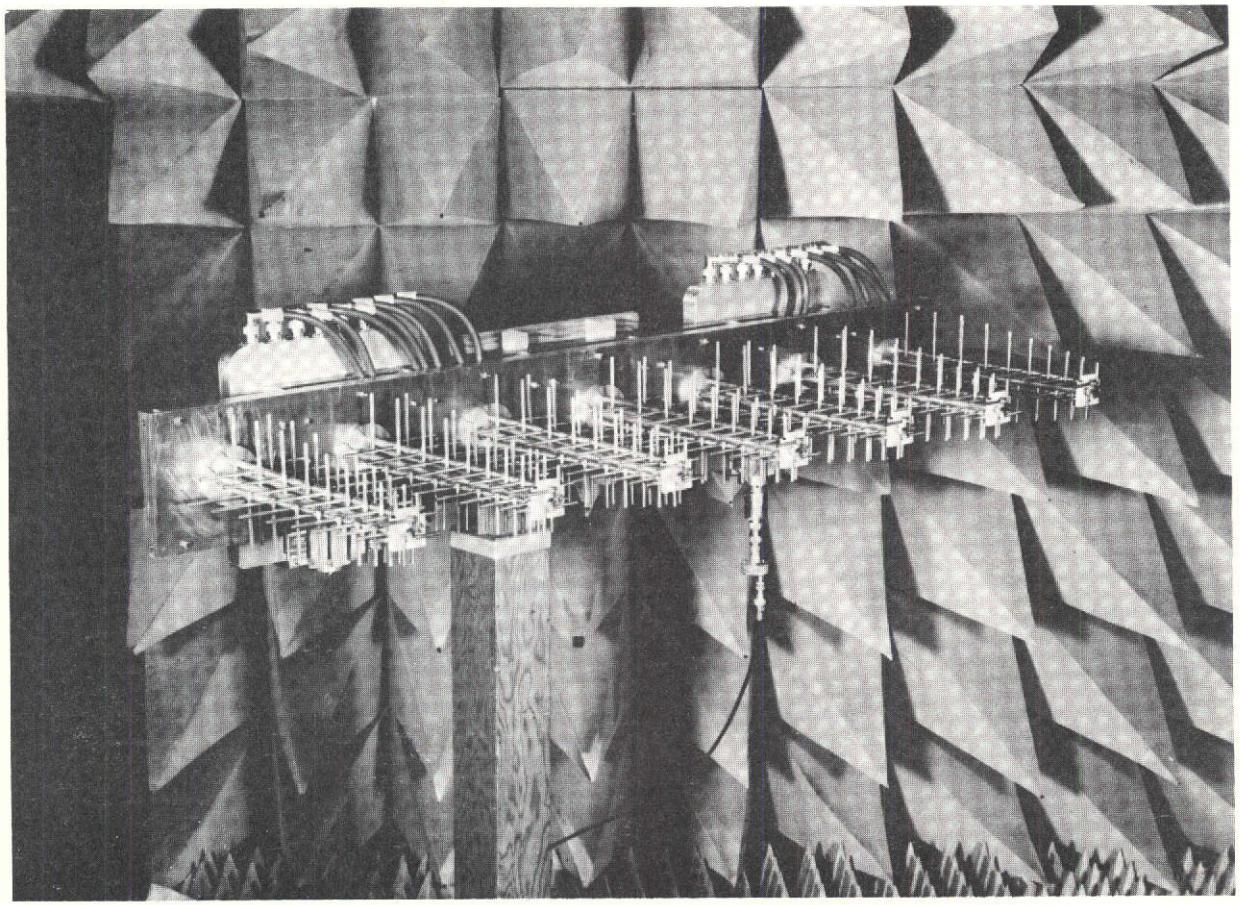

FIGURE 4. DUAL-POLARIZED 7-ELEMENT LOG-PERIODIC ARRAY ASSEMBLY (L-BAND)

An X-band antenna developed on an earlier Air Force contract was chosen for use in this program because of its small physical size and its cross-polarization isolation. The only penalty connected with its use (instead of the antenna used to gather data on the previous NASA effort) is a decrease in one-way gain of about 3 db. Details of the X-band antenna are presented in Appendix B.

TABLE I. DUAL-FREQUENCY RADAR ANTENNA CHARACTERISTICS

	L-Band	X-Band
Operating frequency	1250 MHz	9350 MHz
	+50 MHz	+100 MHz
Side lobe level (relative to main lobe)	- 13 db max.	- 13 db max.
Power (maximum)	50 Kw	50 Kw
Aperture width	5 feet	5 feet
Aperture height	8 inches	4 inches
Polarization isolation	19 db	23 db
Match (VSWR)	<1.5	<1.4

4
OPTICAL DATA PROCESSING

Three possible techniques for optically processing L-band radar data were investigated. Each of these involved a tracking processor in either a tilted-plane or tilted-lens configuration.

The first and most involved method considered requires the generation of an intermediate data film. For this method, a tilted-plane processor would be set up in its normal configuration, but with an over-compression factor α. The processor would be used to (1) remove tilt, astigmatism, and possibly range curvature present in the original signal film and (2) produce a new corrected signal film by holographic techniques. This new intermediate film could then be processed to produce output imagery with a relatively simple optical system which provides basically only a differential magnification in the two dimensions.

For the tilted-plane processor, the general equation for tilt angle is:

$$\sin \theta = \frac{\lambda_r}{2q \lambda_L \alpha^2} \left(\frac{\alpha^2 K^2}{\alpha^2 K^2 - 1} \right) \qquad (1)$$

where:

θ = the angle from the normal at which the input data film is tilted

λ_r = the radar wavelength (~300 m at L-band)

λ_L = processor light wavelength ($\approx 0.6 \times 10^{-3}$ mm)

q = the range dimension packing factor on the input signal film

K = aspect ratio on the input signal film

$\alpha = K_1/K$

K_1 = actual demagnification through the optical processor

If the parameters of the L-band radar are substituted into equation 1, it can be shown that practical solutions exist when $\alpha >> 1$. Because of optical aberration, θ should be no greater than 30°.

A potential problem associated with tilting the input data film plane is the aberration generated by off-axis illumination of the recorded range pulse. The predominant aberration here is coma and its magnitude Δ_c can be calculated from the following equation:

$$\Delta_c = \frac{A^2 \sin \theta}{\alpha \lambda_L f_o^2} \qquad (2)$$

where:

A = half-range zone-plate aperture

f_o = focal length of the tilted zone plate

The zone-plate focal length is:

$$f_o = \frac{v^2 \tau \cos^2 \theta}{B \lambda_L} \qquad (3)$$

where:

v = sweep velocity (recording)

τ = radar chirp pulse length

B = radar signal bandwidth

For the system considered, the effect of this aberration is shown in Fig. 5, which shows an intensity plot of diffracted light from a zone plate tilted 10° off axis. Using the L-band recording parameters, it can be shown that the aberration for this plot is about 0.63λ. The side lobe level is down about 5 db instead of the normal 13.5 db. If the radiated radar pulse length is reduced from 3.0 microseconds to 1.5 microseconds, the aberration will be reduced to 0.32λ and it will appear as in Fig. 6 (the intensity plot for a 5° off-axis zone plate). In this case, the side lobe level is down about 7 db.

Range side lobes will experience a further reduction due to recorder weighting. By proper focusing, this side lobe energy can be averaged over many side lobes so as to reduce the peak level of any one lobe. If the bandwidth were reduced by a factor of two, the aberration would be reduced by a factor of four. Finally, by the use of elliptical apertures in the frequency plane of the processor, the energy can be distributed over a larger area to further reduce the average intensity of the side lobes. An actual point target should appear similar to the target image shown in Fig. 7, which illustrates the effects of various amounts of aberration.

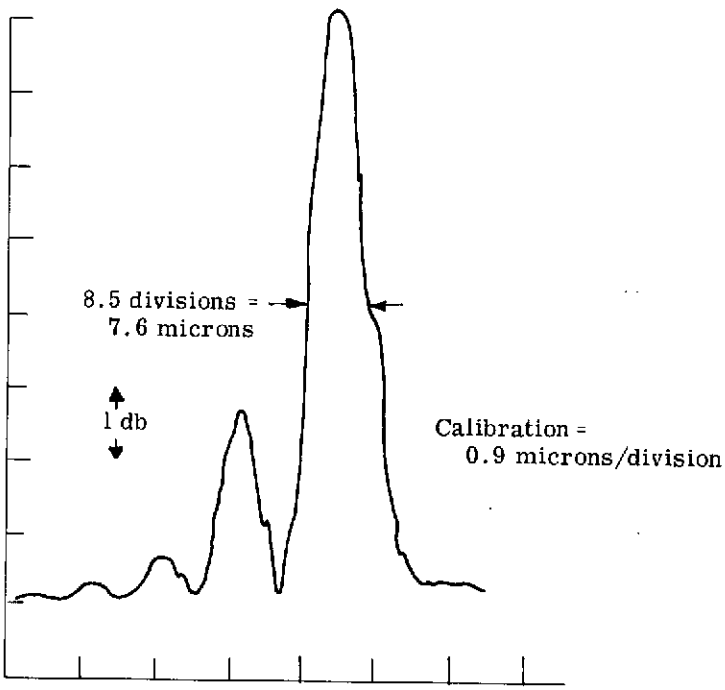

FIGURE 5. AZIMUTH SCAN POINT TARGET 10^{o} OFF AXIS

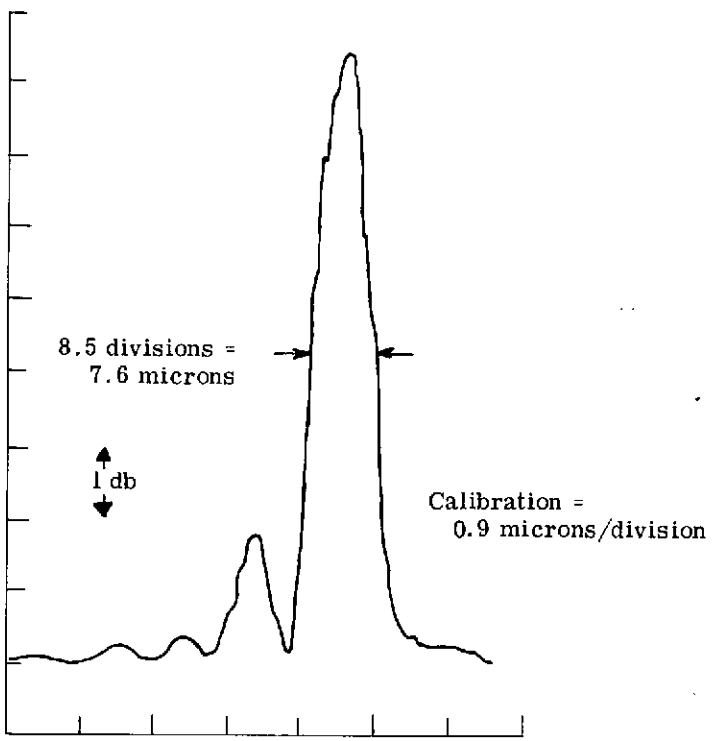

FIGURE 6. AZIMUTH SCAN POINT TARGET 5^{O} OFF AXIS

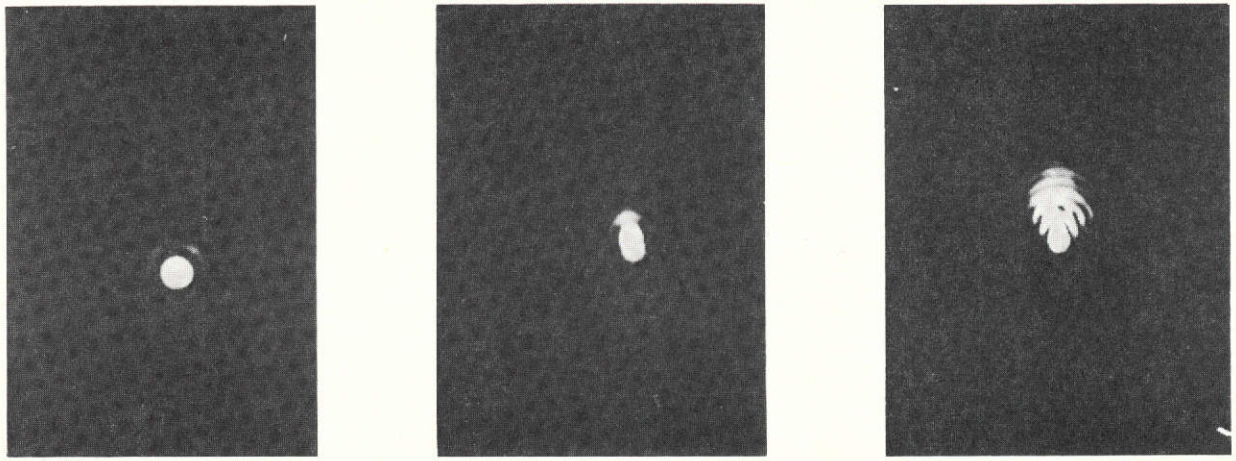

$\Delta_c = 0\lambda$ (a)

$\Delta_c = 0.25\lambda$ (b)

$\Delta_c = 0.95\lambda$ (c)

FIGURE 7. POINT TARGET OUTPUT IMAGE WITH VARIOUS AMOUNTS OF OPTICAL ABERRATION

The original data film has some spatial bandwidth and this would be increased by the factor α on the intermediate film. However, the processor and available recording films could handle these bandwidths with little or no degradation of the recorded radar signals.

A possible disadvantage of this processing method is the existence of the intermediate step. This step provides a signal film which contains all the radar data and which could be used either (1) to view the radar image in great detail using a very simple optical system, or (2) to produce normal output image films with the expenditure of some additional data processing time. Viewing the output image provides undiminished dynamic range and some flexibility of image processing. However, the present contract has no provision for supplying a viewing system. Because of this consideration, the two-step approach was abandoned and effort was concentrated on one-step systems.

A second possible processing system is the tilted-cylinder processor. In this case, the tilted azimuth input plane is demagnified sufficiently to allow the tilt angle to be handled easily. The main parameters are determined by applying the equation for this reduced tilt angle:

$$\tan \Phi = \left(\frac{f_3}{f_2}\right)^2 \quad \frac{\lambda_r}{\alpha \lambda_L} \quad \frac{q}{p^2} \tag{4}$$

where:

Φ = the angle from the normal at which the cylindrical lens is tilted

f_3/f_2 = demagnification ratio

p = the azimuth dimension packing factor on the input signal film

Because of the aberrations which occur when a tilted cylindrical lens is used in an optical system, it is desirable that the tilt angle Φ be as small as possible. A typical rule-of-thumb for this type of processor is that $\Phi \leq 10^{o}$. The terms f_3 and f_2 are lens focal lengths and their ratio $\left(\frac{f_3}{f_2}\right)$ is the demagnification ratio. Based on optical considerations, this ratio should be no smaller than absolutely necessary, and it is best that $f_2 \leq 4\, f_3$. For the desired cross-range resolution, the azimuth bandwidth necessary is easily within the state-of-the-art of recorder design.

The drawbacks of this processing method occur in the processor itself. One problem is the demagnification required. The system requires a large total azimuth bandwidth which is somewhat higher than desirable when using an optical system which includes a tilted cylindrical lens. This lens will invariably introduce some aberrations and care must be taken that these do not limit the resolution.

A third processing method that was considered involves a somewhat unusual application of the tilted-plane processor concept. Taking $\alpha = 1$, in equation 1, that equation becomes:

$$\sin \theta = \frac{\lambda_r}{2q\, \lambda_L} \left(\frac{K^2}{K^2 - 1}\right) \tag{5}$$

Substituting the parameters of the L band radar:

$$\frac{\lambda_r}{2q\,\lambda_L} = 2.5$$

Thus, it can be seen that:

for K = 1, the angle is indeterminate

for K > 1, the minimum value of the right side of the equation is > 2.5 and there is no solution for sine θ

for $0 \leqq K < 1$, the value ranges from 0 to very large negative values

The last of the three conditions provides the only region where valid solutions for θ exist; it can be shown that this region is $0 \leqq K \leqq 0.535$.

To describe further this processing concept, refer to Fig. 8. Planes P_1 and P_3 are the normally vertical input and output planes. Plane P_2 is the azimuth input plane caused by the range-dependent azimuth focal lengths and is displaced an angle β from P_1. Planes P_1^1 and P_4 are the titled film planes (input and output), i.e., P_1^1 is the plane P_1 is tilted into to cause the range and azimuth planes to coincide at the output. P_2^1 is the new plane of azimuth focus caused by the tilt of P_1 into P_1^1. It is seen that the azimuth plane (P_2^1) is not tilted as much as the range plane (P_1^1). After the image is passed through a telescope with a magnification larger than one, the range and azimuth planes can be made coincident. For the L-band case, if tilt angles as great as 30^o are allowed, the necessary value for K can be calculated easily.

It was determined for the system under consideration that bandwidths, film drive velocities, and available optical components for this type of processor were all compatible. This system appears to be superior to the other two proposed systems both in terms of access time and potential optical performance.

Consideration was given to the range curvature problem in the recorded L-band radar data. Although this problem was not extensively analyzed, it was judged that range curvature correction is unlikely to be needed over the proposed mapping interval. If such correction should be required, it probably could be implemented in any of the three processor types considered by tne use of either amplitude or phase correction filters. The theory behind these filters is already well developed; thus, it is felt that range curvature is a soluble problem.

5
OUTPUT IMAGERY

After constructing the L-band equipment and installing it in the aircraft, several local test flights were made to demonstrate the operation of the L- and X-band imaging system. In addition to these local flights, twenty image-gathering flights were made in 1971 over three test sites in Kansas and California. The areas imaged were (1) an agricultural region north of

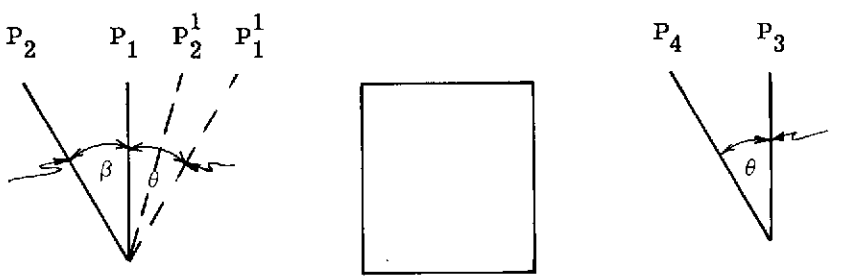

FIGURE 8. ANAMORPHIC OPTICAL PROCESSOR

Holcomb in Finney County, Kansas, (2) Pisgah Crater, Lavic Lake, and the old lava flows in San Bernardino County, California, and (3) the Mono Crater area in Mono County, California. L- and X-band radar images were obtained with both parallel and cross-polarization. Some of the radar images obtained from these flights were degraded for various reasons, including electronic equipment malfunction and navigational errors that displaced the imaged swath from the desired target terrain. However, by repeating some of the flights, useful images were obtained of all target areas. These images illustrate all the desired conditions of polarization and wavelength. Table II shows the record of the system during this period of operation at remote sites.

Figure 9 shows radar imagery of a portion of the Finney County agricultural area and illustrates the effects of the various polarizations and frequencies made available by the dual-frequency and dual-polarization radar system. Figure 10 shows radar imagery of the Pisgah Crater area in San Bernardino County.

TABLE II. REMOTE SITE OPERATION RECORD

Location	Finney County				San Bernardino County				Mono County			
Radar Band	L		X		L		X		L		X	
Radar Transmitter	H	V	H	V	H	V	H	V	H	V	H	V
Passes Started	5	4	4	6	14	11	21	17	4	6	4	5
Passes Aborted	0	0	0	0	1	1	1	1	0	1	0	0
Passes Complete (no target image)	0	0	1	3	0	0	0	0	0	0	0	0
Passes Complete (with imagery)	5	4	3	3	13	10	20	16	4	5	4	5

No image interpretation task was included in this contract and no ground truth information about the target areas was collected under the contract; therefore, no extensive study of the effects of wavelength or polarization on the utility of the data was possible. However, optical views of the target areas were obtained from aerial photographs taken from the radar aircraft during the image-gathering flights. Quick comparisons were made between several aerial photos and the corresponding radar image samples and some differences were observed as a function of wavelength and polarization.

6
CONCLUSIONS

A number of conclusions can be drawn from the results of this contract:

a) As a purely technological conclusion, we found that the frequency conversion approach

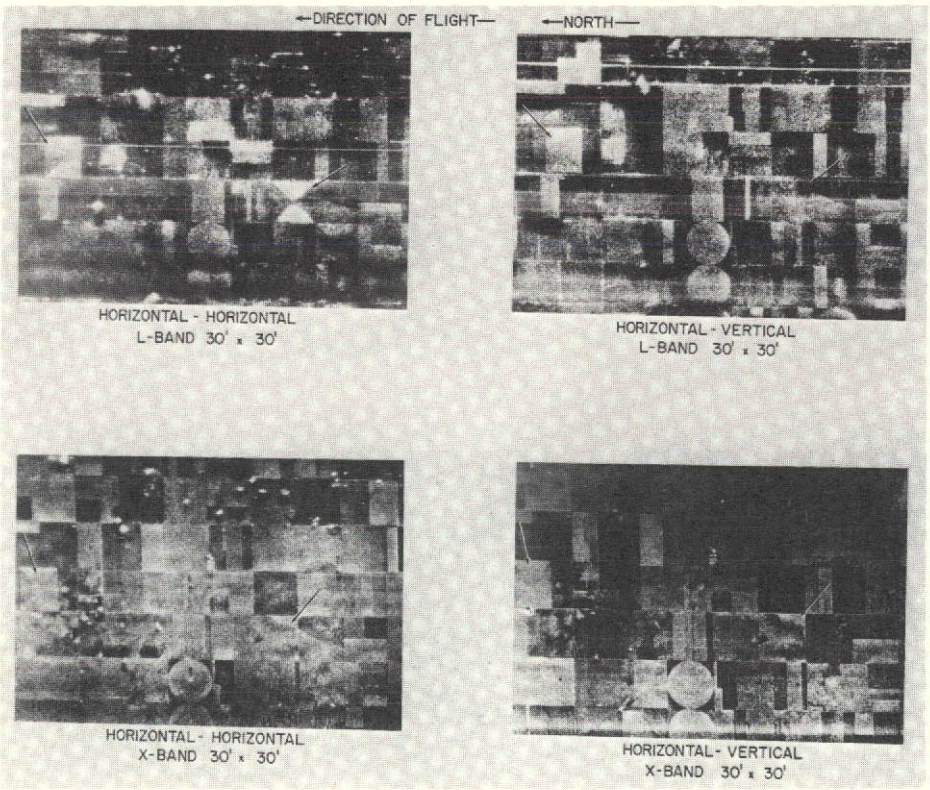

FIGURE 9. FINNEY COUNTY IMAGERY

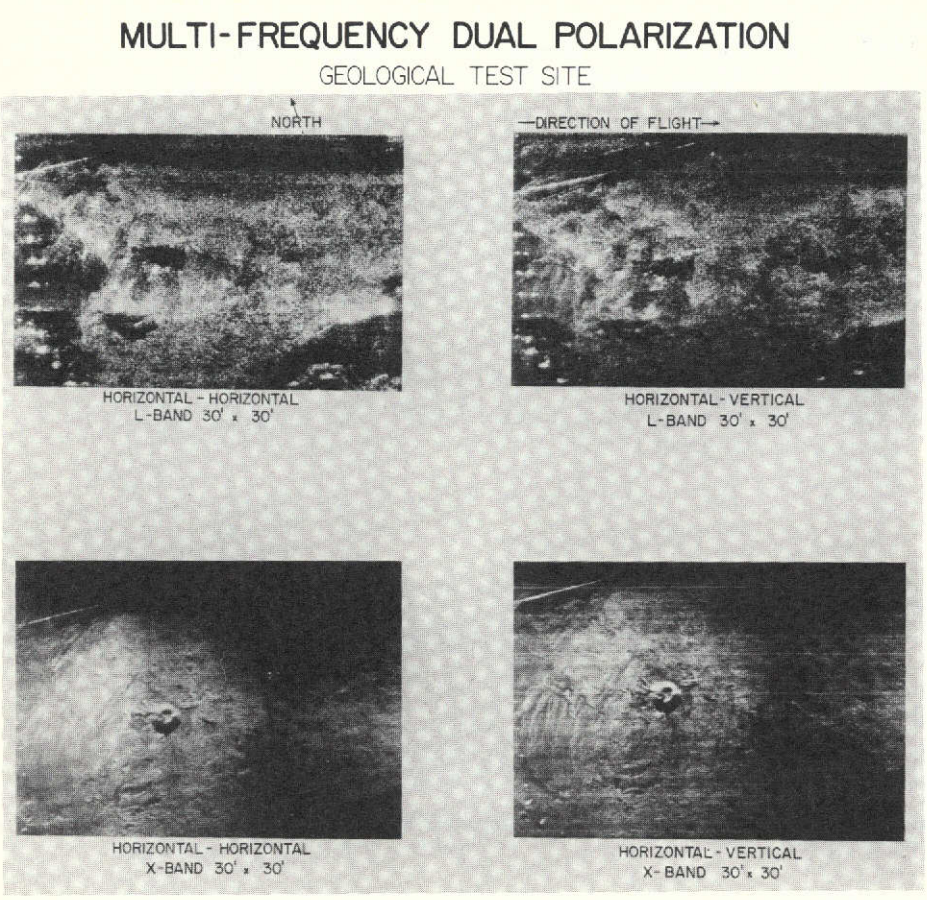

FIGURE 10. PISGAH CRATER IMAGERY

to implementing additional spectral channels on a SAR appears workable in general, and was specifically found to be workable for the X/L combination.

b) On the operational level, we had problems (such as X-band radar circuit unreliability, motion compensation unreliability, and navigational difficulties) with the equipment in the Michigan C-46 aircraft resulting in inadequacies in the embryo X/L system which made it unsatisfactory as a data source for geoscience users.

c) On the scientific level, the textural and spectral response differences in the various images appeared, on the basis of visual examination, to offer promise for radar as a remote sensor, but their true applicability would need to await a systematic examination incorporating accurate ground-truthing and machine processing of the data.

7
RECOMMENDATIONS

The conclusions of Section 6 leads us directly to recommendations for further work in the areas of multispectral radar.

a) It is recommended that modifications be made which improve the reliability of the basic X/L airborne system to the point where it can be employed as a data-gathering radar system for geoscience users.

b) It is recommended that the navigational capabilities of the airborne system be improved so that the weather and time of day do not severely affect its data-gathering capability.

c) It is recommended that the dual-frequency radar system be modified to provide simultaneous operation at the two frequencies. This would reduce data-gathering time and cost, but, more importantly, it would provide radar imagery having greater scientific value. When data are gathered at the two frequencies on separate passes, differences in surface reflectivity due to the wavelength difference are not separable from those due to slight aspect changes or changes in the terrain region itself between passes.

d) Finally, after the modifications suggested above have been performed, it is recommended that the system be used in a well-designed experimental program to acquire scientific data of sufficiently high quality to permit a thoughtful evaluation of the applicability of multispectral imaging radars to earth resource survey missions.

APPENDIX A
L-BAND ANTENNA

The VSWR characteristics of the L-band corporate feed structures are shown in Table III.

The horizontally and vertically-polarized elements were nested together in one package, as shown in Fig. 11.

A typical set of impedance data for a single dual-polarized element is shown in Fig. 12. These data exhibit a VSWR of 1.4:1 or less over a substantial portion of the frequency band. To insure adequate receiver protection, it is necessary for the VSWR to be less than 1.5:1 (corresponding to a power reflection coefficient of less than 0.04). The above impedance matching has been achieved by employing a series matching section of the proper impedance value.

TABLE III. VSWR CHARACTERISTICS FOR DUAL-POLARIZED 7-WAY POWER DIVIDERS

Frequency	Power divider for horizontal array (VSWR)	Power divider for vertical array (VSWR)
1215 MHz	1.12	1.14
1235 MHz	1.06	1.10
1255 MHz	1.02	1.08
1275 MHz	1.06	1.08
1295 MHz	1.14	1.14
1315 MHz	1.20	1.18

The isolation between the transmitter port and the receiver port of the dual-polarized L-band antenna was measured for the dual-polarized element. These data are tabulated in Table IV. To insure that adequate reciever protection is provided, it is necessary for this port-to-port isolation to be at least 14 db. From Table IV, it appears that the isolations should be no less than 30 db in the frequency band of interest.

TABLE IV. HORIZONTAL PORT TO VERTICAL PORT ISOLATION FOR MODEL B - SN2 TESTED 10-20-70

1215 MHz	-	22.7 db
1235 MHz	-	24 db
1255 MHz	-	24.7 db
1275 MHz	-	24 db
1295 MHz	-	26.7 db
1315 MHz	-	31.6 db

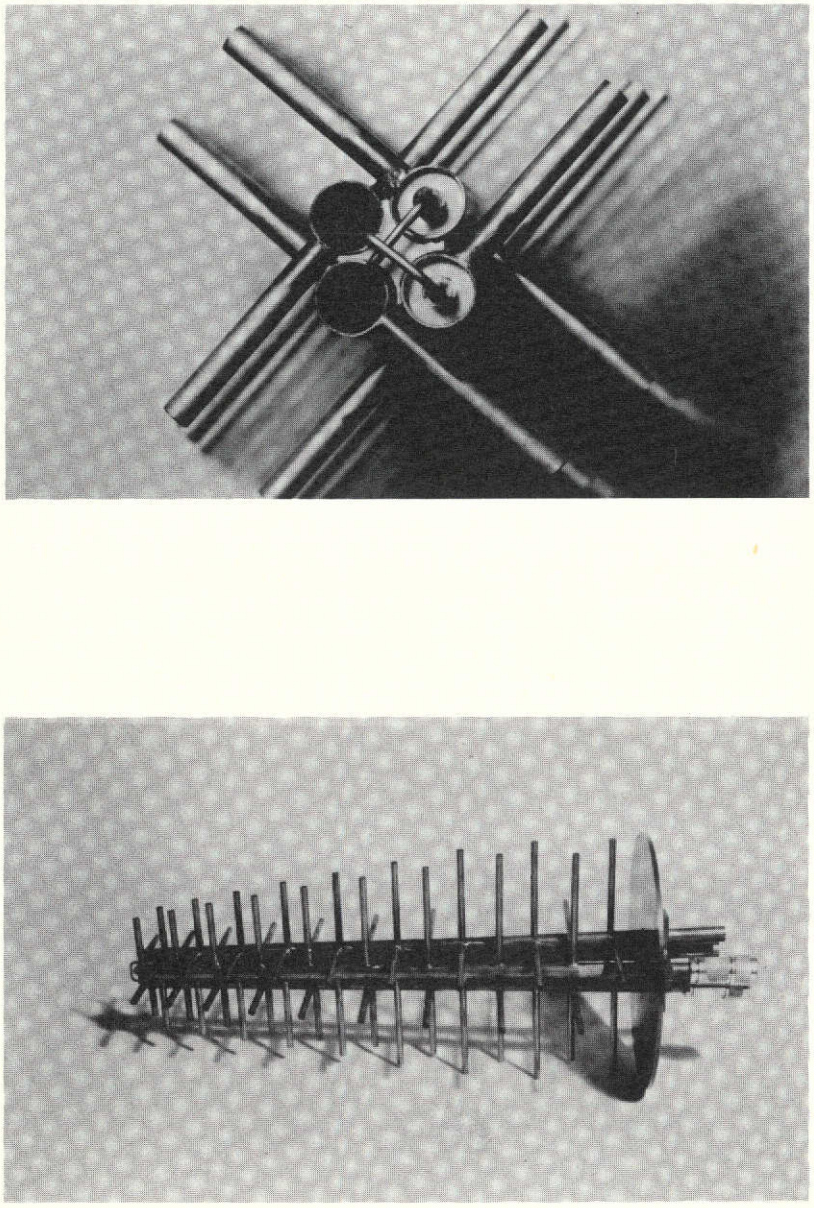

FIGURE 11. DUAL-POLARIZED LOG-PERIODIC ARRAY (L-BAND)

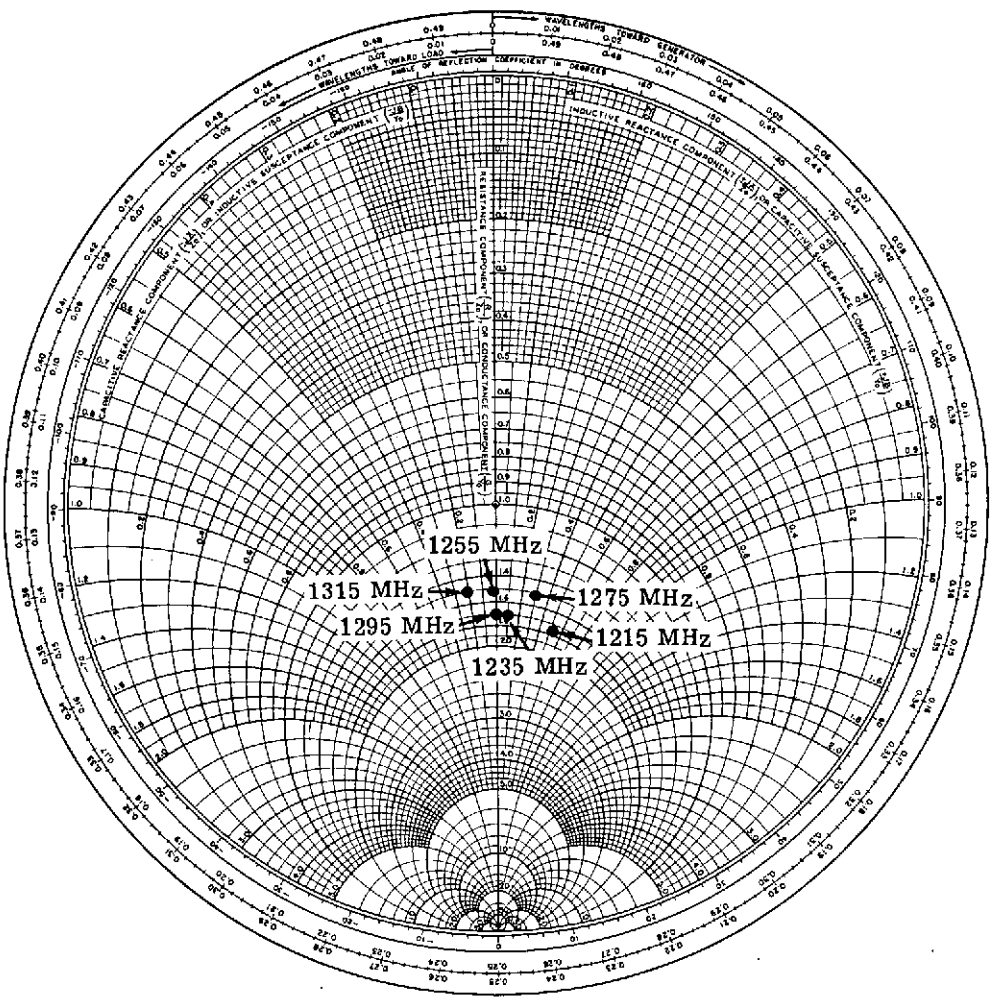

FIGURE 12. IMPEDANCE PLOT FOR A SINGLE DUAL-POLARIZED-LOG PERIODIC ANTENNA (L-BAND)

Both the horizontally and vertically-polarized arrays are excited with a uniform amplitude and phase distribution. The antenna gain of each array was measured to be 16.5 db above an isotropic source. Typical parallel-polarized and crossed-polarized array patterns are shown, respectively, in Figs. 13 and 14.

APPENDIX B
X-BAND ANTENNA

The X-band antenna consists of two slot arrays; each array, in turn, is made up of four sub-arrays. The two slot arrays feed into a common parallel-plate region such that they have a common radiating aperture (Fig. 15). The two arrays are isolated from each other through the use of metallic gratings which are oriented so as to cause energy from the horizontally-polarized array to be rejected from the vertically-polarized array, and vice versa. The four sub-arrays of each major array configuration are interconnected through a corporate feed structure.

The horizontally-polarized array employs inclined-edge shunt slots in the narrow face of the retangular waveguide. This array radiates into a parallel-plate region which resembles a mitered H-plane 90° bend (as seen from the end view in Fig. 16). The mitered wall is replaced with a wire grid structure. The grid structure is constructed with stainless steel drill-rod which is stretched the entire length of the array (~60"). The diameter and spacing of the grids were chosen to provide about 25 db isolation of the horizontally-polarized wave from the vertically-polarized array. The vertically-polarized array employs longitudinal shunt slots in the broad face of the rectangular waveguide. This array radiates into a parallel-plate region of the horn configuration. Part of the wall of the parallel-plate region is composed of another grating structure. This structure was constructed from the broad face of X-band rectangular wave-guide and runs the entire length of the array. Slots were milled in the wall of the guide perpendicular to the axis of the guide to form the grating. Again, this grating was designed to provide 25 db isolation of the vertically-polarized wave from the horizontally-polarized array and yet allow the horizontally-polarized wave to pass through without attenuation.

Figure 17 shows the arrangement of the four sub-arrays to form the two five-foot arrays of the antenna. The four sub-arrays of each major array are interconnected with a waveguide. corporate feed structure. Figure 18 shows the typical construction of a section of the corporate feed structure. Within the individual corporate feed sections, there are septums, irises, and quarterwave transformers used to provide impedance matching of the sub-arrays and feed structures. These devices will be discussed in detail later.

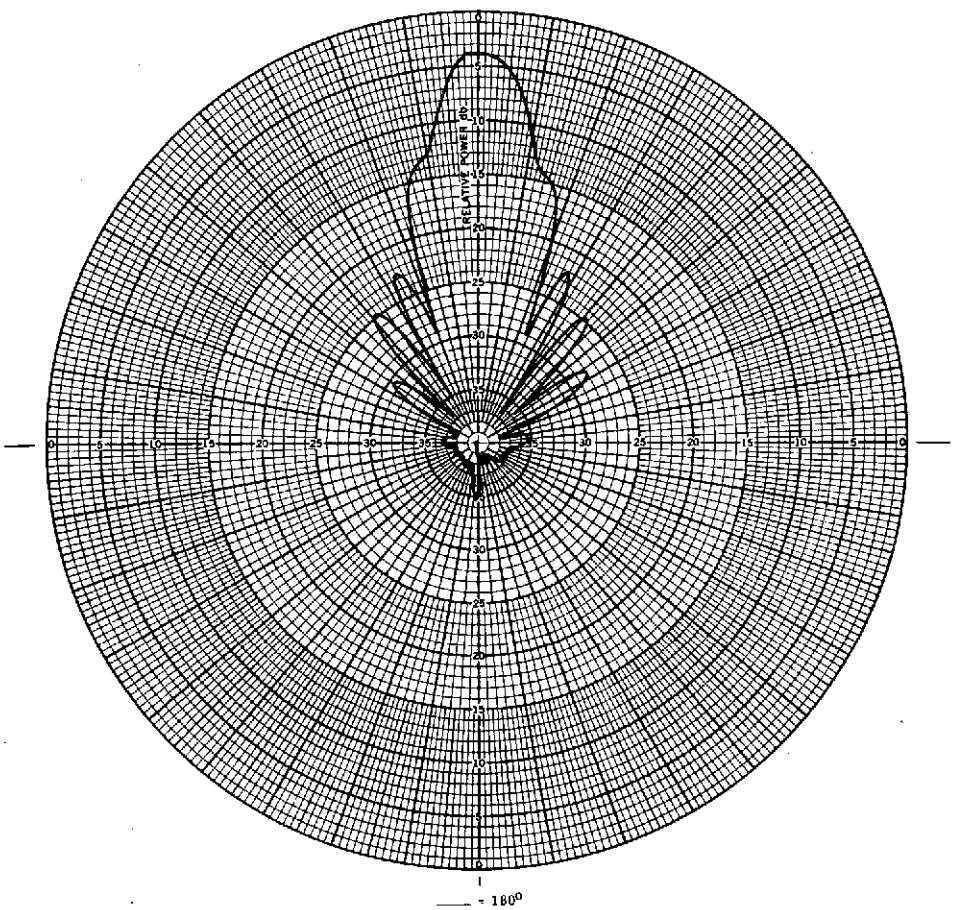

FIGURE 13. PARALLEL-POLARIZED PATTERN
FOR 7-ELEMENT LOG-PERIODIC ARRAY (L-BAND)

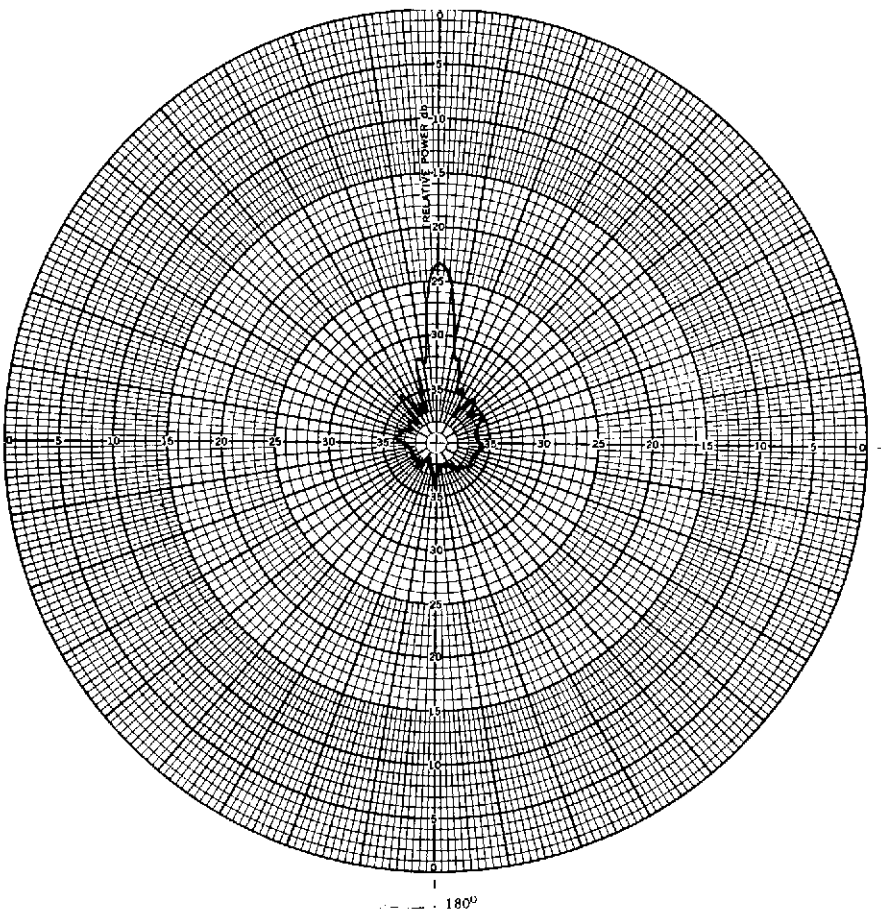

FIGURE 14. CROSS-POLARIZED PATTERN FOR
7-ELEMENT LOG-PERIODIC ARRAY (L-BAND)

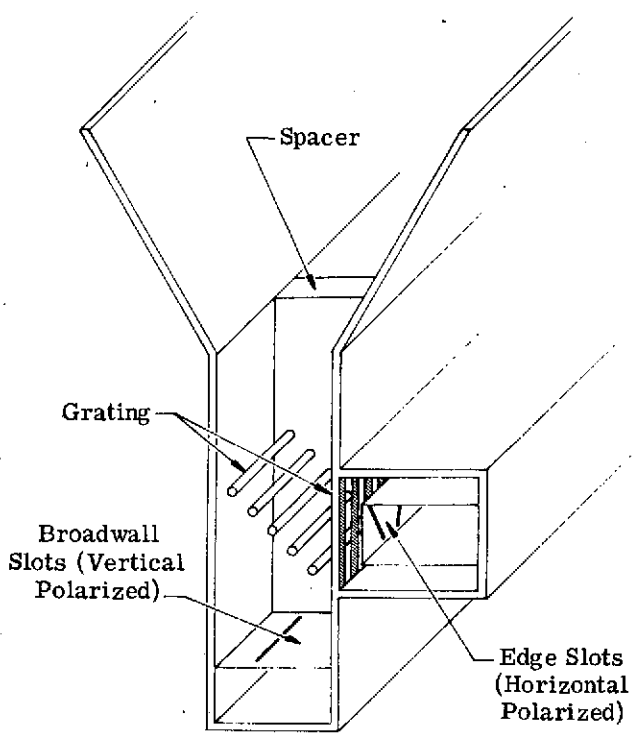

FIGURE 15. DUAL POLARIZED SLOT ARRAY (X-BAND)

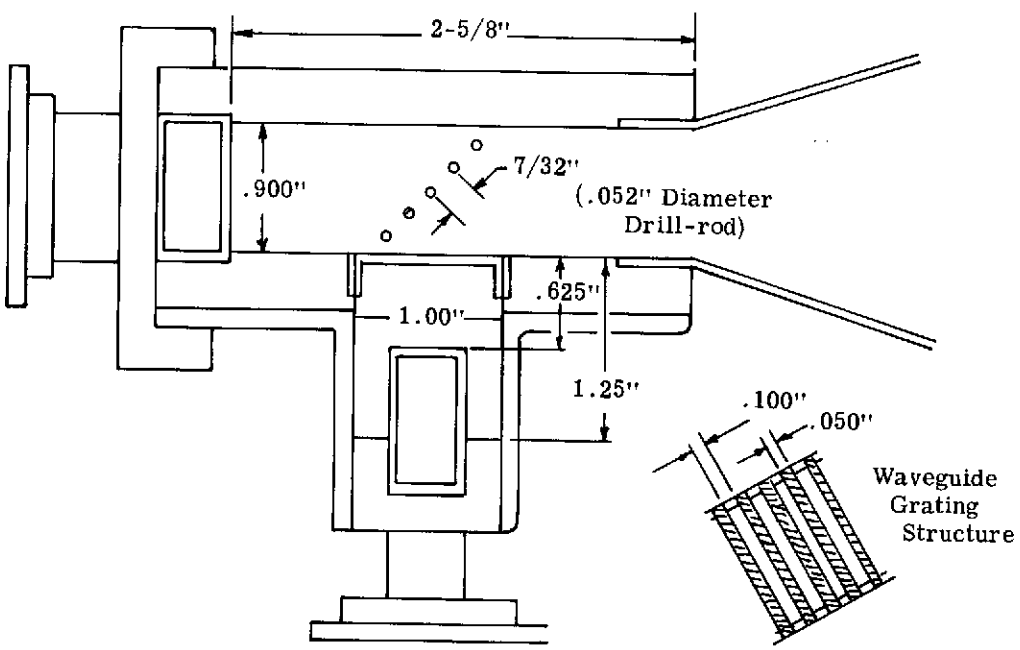

FIGURE 16. END VIEW OF DUAL POLARIZED SLOT ARRAY SHOWING THE CRITICAL DIMENSIONS (X-BAND)

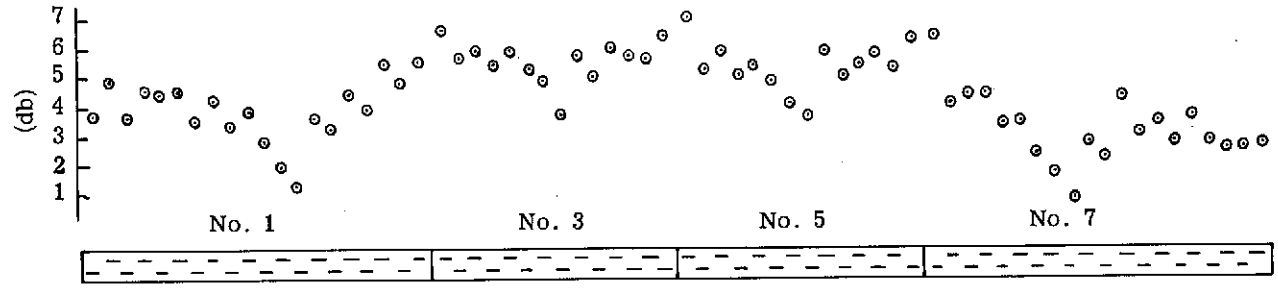

A. Broadwall shunt slot array arrangement and relative slot coupling

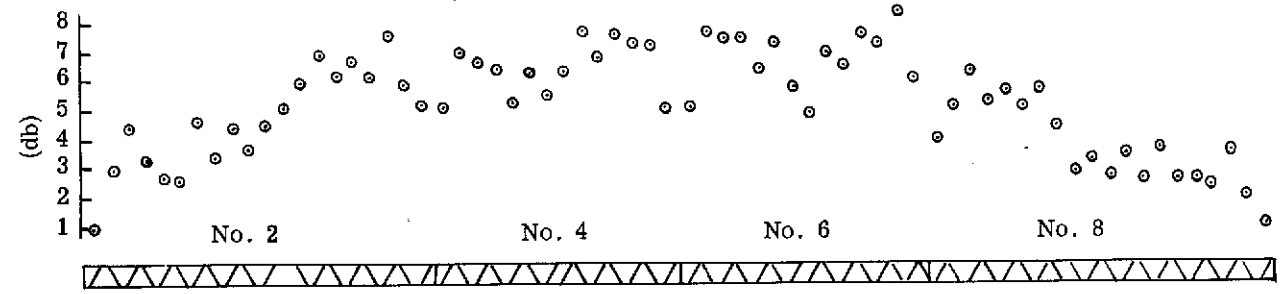

B. Edge shunt slot array arrangement and relative slot coupling

FIGURE 17. ARRANGEMENT OF THE FOUR SUB-ARRAYS TO FORM THE LARGE FIVE-FOOT ARRAY, AND SLOT COUPLING AMPLITUDE DISTRIBUTION (X-BAND)

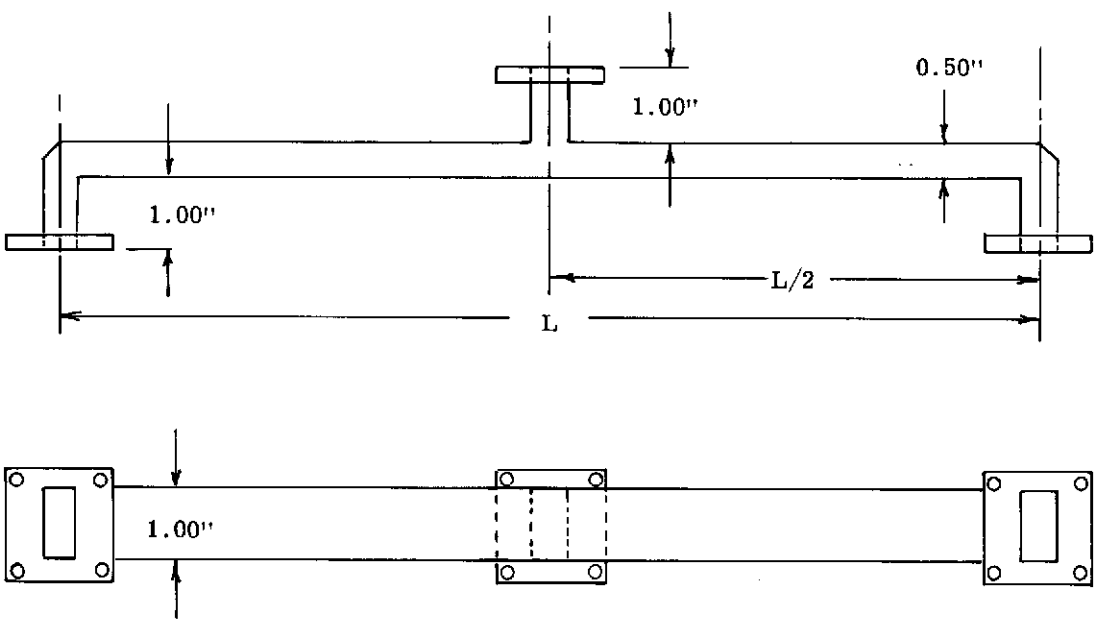

FIGURE 18. TYPICAL CONSTRUCTION OF WAVEGUIDE CORPORATE FEED STRUCTURE (X-BAND)

To achieve the desired azimuthal half-power beamwidth and side lobe levels, an aperture distribution approximating a cosine function on a pedestal was used. To determine if the correct slot-coupling was maintained, the energy coupled from each slot was measured with the aid of a surface-current measurement facility. The results are shown in Fig. 17, which indicates that approximately proper amplitude distribution was obtained.

The parallel-plate horn configuration was constructed of machinable aluminum and the parts black-anodized. The configuration was then assembled with ny-lok machine screws; the nylon inserts in these screws prevent the screws from loosening due to vibration in the airborne application.

Before radiation pattern and coupling data could be obtained, it was necessary to assemble and impedance match the corporate feed structures. This was required because the large mismatches that could occur within the corporate feeds might cause moding or phase variations; these, in turn, might result in improper addition or cancellation of the received signal.

The impedance matching of the array was performed by means of inductive irises and/or quarter-wavelength impedance transformers inserted into the waveguide corporate feed structures at calculated proper locations.

Table V shows the VSWR's of the various corporate feed inputs after matching. The final VSWR's were approximately 1.3:1 or less over the frequency range of 9.25 to 9.45 GHz.

TABLE V. VSWR'S FOR CORPORATE FEED INPUTS AFTER IMPEDANCE MATCHING

Frequency	Broadwall	Slot Array	Feed Nos.	Edge Shunt	Slot Array	Feed Nos.
(GHz)	No. 1-3	No. 5-7	No. 1-3-5-7	No. 2-4	No. 6-8	No. 2-4-6-8
9.25	1.38	1.43	1.12	1.27	1.18	1.14
9.3	1.40	1.16	1.30	1.22	1.31	1.28
9.35	1.18	1.20	1.18	1.16	1.30	1.23
9.4	1.18	1.29	1.14	1.20	1.16	1.17
9.45	1.27	1.29	1.29	1.30	1.21	1.30

After the final impedance matching was accomplished, radiation pattern and cross-coupling measurements were made. The edge shunt array (horizontal polarization) and the broadwall shunt array (vertical polarization) were found to exhibit side lobe levels which were below the main beam level by approximately 10 db or more and azimuth beamwidths of 1-1/2 degrees. The cross-coupling data for the edge shunt and broadwall shunt arrays are respectively 26 and 23 db below the parallel-polarized component level. The antenna elevation beamwidth is seen in Fig. 19 to be about 23°. Unusually high side lobes were observed at $\pm 45^{\circ}$ for the broadwall shunt array at 9.25 GHz; these are thought to be caused by reflections from the antenna end plates. It is believed that removal of the upper portion of the end plates would reduce or eliminate these side lobes. However, removal of the plates would also reduce the rigidity of the horn structure; since this rigidity is needed for airborne applications, their removal was not considered justified.

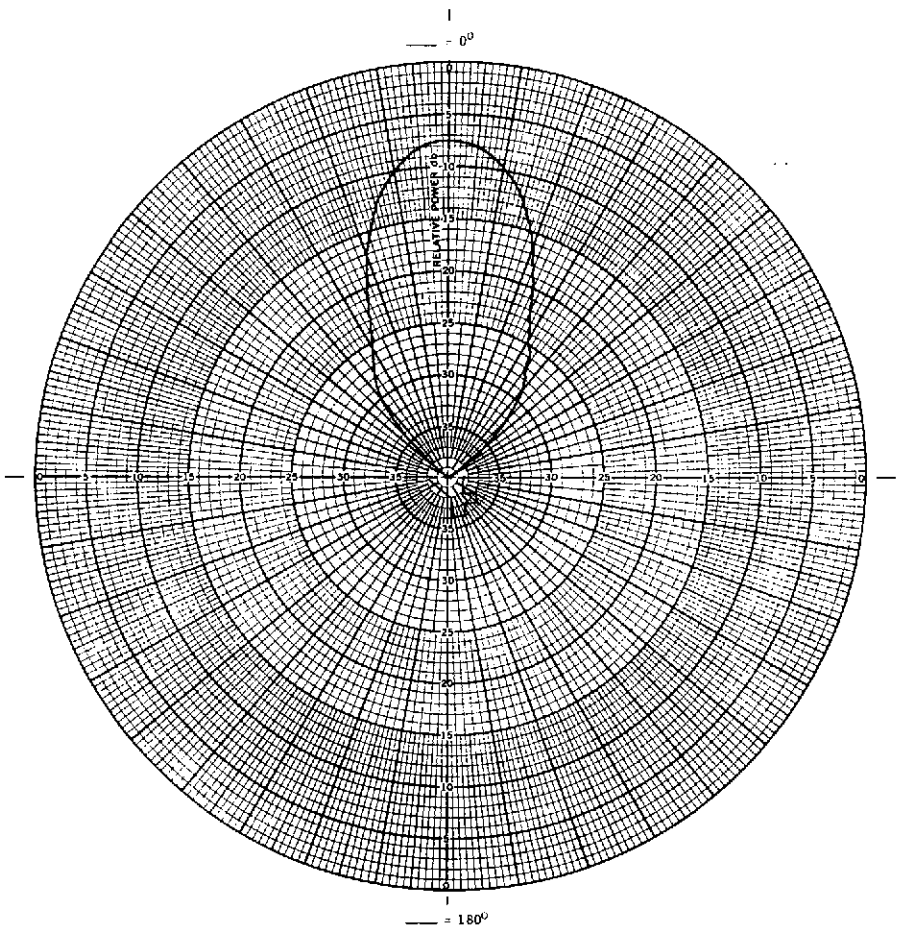

FIGURE 19. ELEVATION RADIATION PATTERN OF THE EDGE SHUNT SLOT ARRAY (9.35 GHz)